Inorganic Chemistry

Article

pubs.acs.org/IC

Electron-Deficient Telluride $Cs_3Cu_{20}Te_{13}$ with Sodalite-Type Network: Syntheses, Structures, and Physical Properties

Wen-Juan Huai,[†,‡] Jin-Ni Shen,[†,‡] Hua Lin,[†] Ling Chen,[†] and Li-Ming Wu*[,†]

[†]State Key Laboratory of Structural Chemistry, Fujian Institute of Research on the Structure of Matter, Chinese Academy of Sciences, 155 Yangqiao Road West, Fuzhou, Fujian 350002, People's Republic of China

[‡]University of Chinese Academy of Sciences, No. 19A Yuquan Road, Beijing, 100049, People's Republic of China

Supporting Information

ABSTRACT: The first sodalite-type telluride, $Cs_3Cu_{20}Te_{13}$, has been successfully synthesized by solid-state reactions. The single-crystal X-ray diffraction data reveal its cubic symmetry and lattice parameters of a = 14.7557(6) Å, V = 3212.8(2) Å^3, and Z = 4. The three-dimensional network is constructed by $(CuTe)_{12}$ tetrakaidecahedra centered by different guest species (either a Cs^+ or a Te^{2-}@Cu_8 cube) extending in a 2 × 2 × 2 supercell with respect to the conventional sodalite. Density functional theory analysis uncovers the unique feature of the p-type metallic sodalite framework accommodating anionic guest species, which agrees well with the experimental metallic electrical conductivity and Pauli paramagnetism.

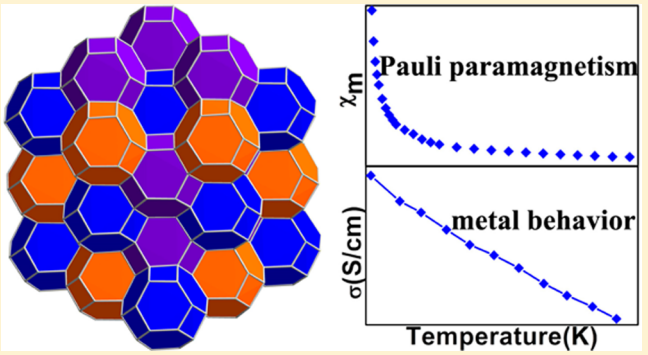

INTRODUCTION

The copper chalcogenide family has attracted considerable attention not only because of their potential applications but also because of their diverse structure chemistry.[1,2] The dimensionality and properties of ternary A/Cu/Q compounds (A = alkali, Q = S, Se, Te) are affected by the alkali cations.[3,4] On the basis of the Zintl rule, these chalcogenides can generally be classified into two categories that are correlated with properties: valence-precise and electron-deficient compounds. The former is the majority, showing semiconducting or insulating properties; the latter is the minority, exhibiting metallic conductivity.[2] The few electron-deficient examples are $Na_3Cu_4S_4$,[5] $NaCu_4S_4$,[6] ACu_4Q_3 (Q = S, Se),[7] $A_3Cu_8Q_6$,[2,8] $K_2Cu_5Te_5$,[9] and $A_3Cu_8Te_{10}$,[10] which are one electron deficient per formula. Interestingly, the valence-precise and electron-deficient compounds are switchable back and forth via chemical doping/substitution; for example, the substitution of one A^+ in p-type metallic $A_3Cu_8Te_{10}$ by one Ba^{2+} generates a valence-precise semiconducting derivative.[10] As usual, the number of tellurides is much less than that of sulfides and selenides; only three electron-deficient tellurides are known, namely, $A_3Cu_8Te_6$,[2,8] $K_2Cu_5Te_5$,[9] and $A_3Cu_8Te_{10}$.[10] From the structural point of view, the majority of A/Cu/Te compounds are two-dimensional layered, whereas a few are three-dimensional (3D) networks, such as $K_4Cu_8Te_{11}$,[11] $K_3Cu_{11}Te_{16}$,[12] and $K_2Cu_2Te_5$,[13] of which the frameworks are built by Cu/Te tunnels that are connected by polyanions of Te_2^{2-} or Te_3^{2-}. The networks of $K_4Cu_8Te_{11}$[11] or $K_3Cu_{11}Te_{16}$[12] can also be viewed as frameworks that are constructed by pentagonal dodecahedron $Cu_8(Te_2)_6$ containing ditelluride edges.

Herein, we report the first sodalite-type telluride, $Cs_3Cu_{20}Te_{13}$, constructed by condensed $(CuTe)_{12}$ tetrakaidecahedra extending in a 2 × 2 × 2 supercell with respect to a conventional sodalite. The density functional theory (DFT) studies point out the features of the metallic 3D sodalite framework accommodating anionic guest species, which agree well with the experimental results of Pauli paramagnetic property and metallic electrical conductivity.

RESULTS AND DISCUSSION

Crystal Structure. $Cs_3Cu_{20}Te_{13}$, crystallizes in the space group $Fm\bar{3}$ with a = 14.7557(6) Å, V = 3212.8(2) Å^3 and Z = 4 according to the single-crystal diffraction analyses. The powder X-ray diffraction data, indicating pure-phased $Cs_3Cu_{20}Te_{13}$ shown in Figure 1, were measured on ground hand-picked crystals. The major structure feature is the novel 3D framework in a sodalite topological linkage that is constructed by condensed 24-atom tetrakaidecahedra, $(CuTe)_{12}$, via strong Cu−Te covalent bonding interactions (Figure 2b,d). Such a tetrakaidecahedron is constructed by four-coordinated apexes of Cu2 at 48h and Te1 at 48h sites, which is reminiscent of the truncated octahedron (known as the sodalite cage) in the sodalite family,[14] for example, the $(SiO_2)_{24}$ cage in $[(C_2H_4(OH)_2)_2][Si_{12}O_{24}]$, in which each apex is a SiO_4-tetrahedron[15] (Figure 2c). The $(CuTe)_{12}$ caged building unit generates the major 3D framework via sharing its six square faces along [100], [010], and [001] directions and eight hexagonal faces along the body diagonal directions (Figure 2d).

Received: February 5, 2014
Published: May 13, 2014

dx.doi.org/10.1021/ic500291v | Inorg. Chem. 2014, 53, 5575−5580

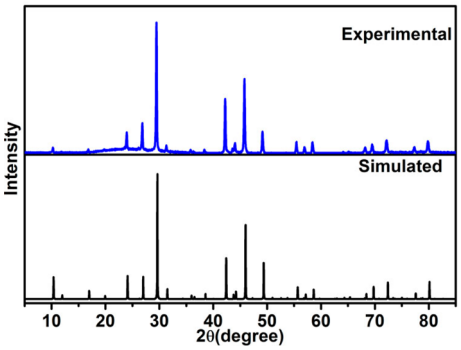

Figure 1. Experimental and simulated X-ray powder diffraction patterns of hand-picked $Cs_3Cu_{20}Te_{13}$ crystals; pure phase is indicated.

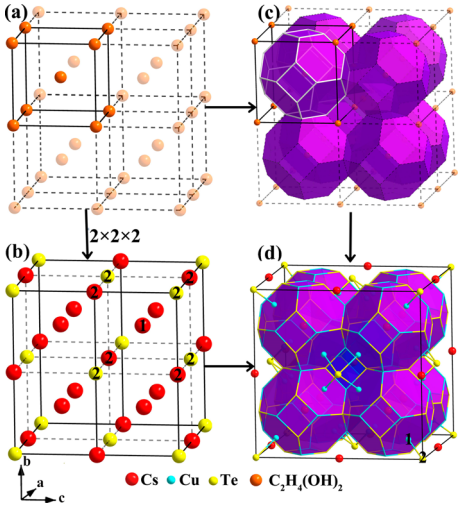

Figure 2. Structure relationship between $Cs_3Cu_{20}Te_{13}$ and a representative of the sodalite family, $[(C_2H_4(OH)_2)_2][Si_{12}O_{24}]$.[17] (a) The CsCl-type substructure of the guest species in $[(C_2H_4(OH)_2)_2]$-$[Si_{12}O_{24}]$. (b) The substructure of the guest atoms in $Cs_3Cu_{20}Te_{13}$: $Cs1^+$ at 4*b* site, $Cs2^+$ at 8*c* site, and $Te2^{2-}$ at 4*a* site. (c) The 3D sodalite framework of $[(C_2H_4(OH)_2)_2][Si_{12}O_{24}]$. Tetrakaidecahedron: $C_2H_4(OH)_2@(SiO_2)_{12}$, note that each apex represents a SiO_4 tetrahedron. (d) The 3D sodalite framework of $Cs_3Cu_{20}Te_{13}$. Tetrakaidecahedron: $Cs1@(Cu2Te1)_{12}$, blue apex: Cu2 atom; yellow apex: Te1 atom. The guest Cu1 and Te2 atoms are numbered. The unit cell is marked by black lines.

Such a linking topology is the same as that in $[(C_2H_4(OH)_2)_2]$-$[Si_{12}O_{24}]$,[15] in which all tetrakaidecahedra are centered by the same organic molecule $(C_2H_4(OH)_2)_2$ adopting a simple CsCl-type arrangement (Figure 2a). But in $Cs_3Cu_{20}Te_{13}$, three types of inorganic centering species are presented; thus, the $Cs_3Cu_{20}Te_{13}$ sodalite-type framework is fully expanded into a 2 × 2 × 2 supercell with respect to that of $[(C_2H_4(OH)_2)_2]$-$[Si_{12}O_{24}]$[15] (Figure 2b vs 2a).

All tetrakaidecahedra in $Cs_3Cu_{20}Te_{13}$ are formed by Cu2−Te1 covalent bonds but are centered by different guest species, either a Cs1 (at 8*c* site) or a Cs2 (at 4*b* site), or a unique 8-fold coordinated Te2 atom (at 4*a* site) serving as the center of the $Cu1_8$ cube, which is further encapsulated by the tetrakaidecahedron (i.e., $Cu1_8$ cube share with $(Cu2Te1)_{12}$ tetrakaidecahedron a common center Te2). These polyhedra are thus denoted as Cage-I, $Cs1@(Cu2Te1)_{12}$; Cage-II, $Cs2@(Cu2Te1)_{12}$; and Cage-III, $Te2@Cu1_8@(Cu2Te1)_{12}$, respectively (Figure 3a). Note that Cu1 locates on the

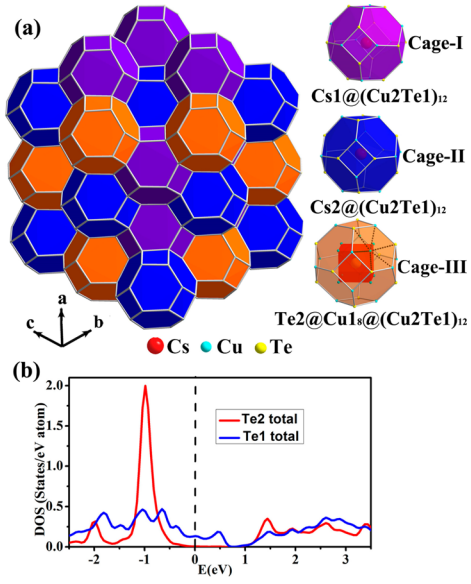

Figure 3. (a) Polyhedral representation of $Cs_3Cu_{20}Te_{13}$. The polyhedron color legend is given on the right. For the sake of clarity, Cu1 atoms on the hexagonal rings of Cage-III are omitted. In the color legend of cage-III, the dotted lines indicate the secondary interactions between Cu1 and the framework atoms. (b) The PDOS of Te atoms indicating the markedly different contributions of the framework Te1 atom and the guest $Te2^{2-}$ anion. Vertical dotted line represents E_F.

hexagonal faces of each Cage-III and shows weak secondary interactions with the framework atoms of Cu2 and Te1. Eight Cu1 atoms form a cube with Cu1−Cu1 edge of 3.042(2) Å without any noticeable interaction. The unit cell contains eight Cage-I, four Cage-II, and four Cage-III polyhedra. Some selected linkages of these cages are illustrated in Supporting Information, Figure S7, such as the [001] extension of Cage-I; the connection of cages II and III via sharing common square along [001]; and the linkage of three type of cages I, II, and III through the hexagonal rings along [111] direction. The partial density of states in Figure 3b clearly illustrates that Te1 (framework atom) and Te2 (guest atom) contribute differently to the electronic structure, as discussed below.

As shown in Figure 4, the framework Cu2 atoms adopt distorted tetrahedral local coordination ($Cu2Te1_4$ tetrahedron) with Cu2−Te1 bonds of 2.586(2)−2.620(2) Å, which match well with those in $Cs_4Cu_8Te_{11}$ (2.556(1)−2.701(2) Å).[11] There are two secondary strong interactions around Cu2 atom (dotted lines, Cu2−Cu1 = 2.634(2) Å).[11] The framework Te1 atoms are also tetrahedrally coordinated by four Cu2−Te1 bonds ranging from 2.586(2) to 2.620(2) Å. Except these, there are two relatively weak secondary interactions around Te1 atom (dotted lines, Te1−Cu1 = 2.7215(7) Å) that are even longer than that of the 8-fold coordinated Te2 atom. The guest Cu1 atoms are 1-fold coordinated with Te2 with strong covalent Cu1−Te2 = 2.635(2) Å, and Cu1 also interacts with the framework atoms (Te1 and Cu2) via secondary interactions that are weaker but cannot be totally ignored (more details below). The 8-fold coordination mode of $Te2^{2-}$ anion is found for the first time; however, it is similar to μ_8-Se in $(H_2en)_{3/2}[Cu_8(\mu_8\text{-Se})(AsSe_4)_{6/2}]$.[16] Tellurium serving as centering species is also seen in $Ge_{79}P_{29}S_{18}Te_6$.[17]

The significance of the sodalite-type $Cs_3Cu_{20}Te_{13}$ lies in that, to date, the sodalite framework is only found in hydrates and oxides,[18] for example, $[(HPF_6)_2][O_{12}H_{24}]$,[19] $[(ClNa_4)_2]$-

dx.doi.org/10.1021/ic500291v | Inorg. Chem. 2014, 53, 5575−5580

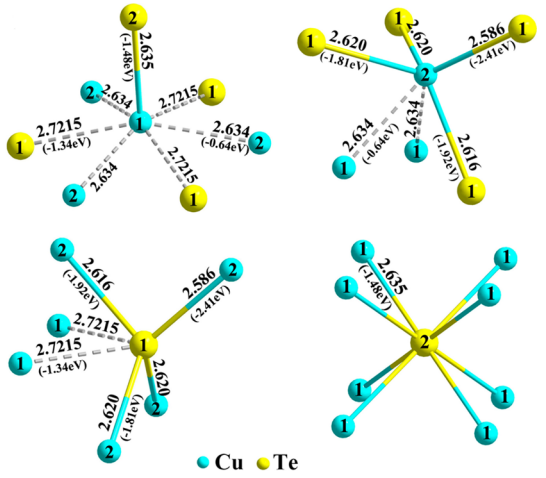

Figure 4. Local coordination environments of Cu1, Cu2, Te1, and Te2 in $Cs_3Cu_{20}Te_{13}$ with bond distances marked. The values in the parentheses are the ICOHP values calculated by LMTO method, by which the bond strength between the same pairs of atoms can be compared.

$[Al_6Si_6O_{24}]$,[20] and $[(C_2H_4(OH)_2)_2][Si_{12}O_{24}]$.[15] According to the Zintl formalism[21−23] and based on the assumption of Cu^+ with d^{10} configuration and Cs^+ and Te^{2-} ions with $5s^25p^6$ configurations, the anionic moiety $[Cu_{20}Te_{13}]^{6-}$ should have six negative charges. Because there are only three Cs^+ cations per formula, $Cs_3Cu_{20}Te_{13}$ is thus three electrons deficient. Then, where these three holes are located is worth asking. This will be addressed below.

Magnetic Property. The polycrystalline $Cs_3Cu_{20}Te_{13}$ exhibits Pauli paramagnetism, indicating a characteristic of metals with a small temperature-independent contribution of 0.00238(1) emu/formula unit at H =1000 Oe. The zero field cooled susceptibility and inverse susceptibility are shown in Figure 5a, which appears identical to the field cooled value under the measurement conditions. The inverse susceptibility (Figure 5 inset) obeys the modified Curie−Weiss law $\chi = \chi_0 + C/(T - \theta)$,[24−26] with Pauli paramagnetism (χ) about 4.93 × 10^{-4} emu mol^{-1}/Cu, Curie constant C = 0.00315(5) emu K/mol, and Weiss constant θ = −6.66(17) K. And the total paramagnetic moment is calculated to be 0.159(1) μ_B/Cu, which is much smaller than the theoretical value of Cu^{2+} ion (about 1.73 μ_B/Cu^{2+}). Therefore, the magnetic behavior of $Cs_3Cu_{20}Te_{13}$ may reasonably be explained as that the Cu atom is monovalent, and some paramagnetic impurities coexist. Similar phenomena are found in $K_2Cu_5Te_5$ with Pauli paramagnetism of about 8 × 10^{-4} emu mol^{-1}/Cu,[9] $Yb_9Zn_{4.03(2)}Bi_9$ with 2.78 × 10^{-5} emu mol^{-1}/Yb,[26] and $Na_3Cu_4S_4$ with 3.75 × 10^{-5} emu mol^{-1}/Cu.[5]

Electrical Conductivity. The electrical conductivity was measured on a cold-pressed pellet of polycrystalline $Cs_3Cu_{20}Te_{13}$ (with 78% of the theoretical density) from room temperature to 495 K to ensure no decomposition occurs (Figure 5b). The electrical conductivity shows an inverse temperature dependence indicating a metal behavior. The room-temperature electrical conductivity (about 2390 S/cm) lies between the values of typical metals and semiconductors and is comparable with that of metallic $KCuLaTe_4$ (1700 S/cm).[27] The metallicity revealed by the conductivity measurement agrees well with the Pauli paramagnetic property and the Zintl formalism discussed above.

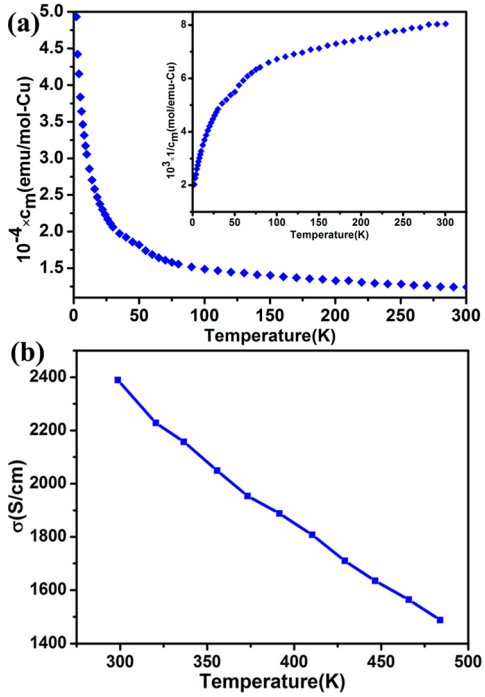

Figure 5. Physical properties of $Cs_3Cu_{20}Te_{13}$. (a) Temperature-dependent magnetic susceptibility. (inset) Inverse susceptibility. (b) Temperature-dependent electrical conductivity measured on a cold-pressed polycrystalline pellet.

Electronic Structure. To further understand the band nature and the transport property of $Cs_3Cu_{20}Te_{13}$, DFT calculations were carried out. As shown in Figure 6, the

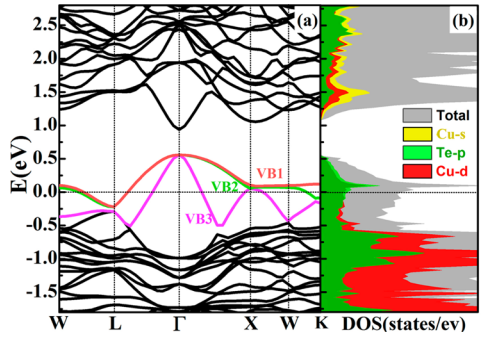

Figure 6. (a) Band structures of $Cs_3Cu_{20}Te_{13}$. The top three valence bands are marked as red (VB1), green (VB2), and pink (VB3). (b) DOS curves of $Cs_3Cu_{20}Te_{13}$. The color region represents the total and partial DOS as marked. The E_F is set at 0 eV.

Fermi level (E_F) of $Cs_3Cu_{20}Te_{13}$ crosses the valence bands (VBs), indicating a metallic feature. And at the VB top slightly above E_F, a visible band gap of 0.5 eV is seen; thus, $Cs_3Cu_{20}Te_{13}$ is expected to be a p-type metallic conductor, which agrees well with the electrical conductivity and the Pauli paramagnetism discussed above. The total (TDOS) and partial (PDOS) densities of states indicate that states near E_F mainly belong to Cu 3d and Te 5p states, on which the three holes of $(Cs^+)_3(Cu^{1+})_{20}(Te^{2-})_{13}$ based on the Zintl formalism should be located.

The conduction bands ranging from 1.0−2.5 eV are dominated by Cu 4s and 3d orbitals. The PDOS of the framework Te1 or the guest Te2 contribute profoundly

dx.doi.org/10.1021/ic500291v | Inorg. Chem. 2014, 53, 5575−5580

differently around E_F (Figure 3b and Supporting Information, Figure S8). The latter contributes sharply at ca. −1.0 eV below E_F and vanishes around E_F, whereas the former spreads across E_F over a large energy range. Thus, the oxidation state on Te2 atom can be assigned as −2. The PDOS integration of copper and tellurium atoms around E_F in the energy range of from −0.05 to 0.1 eV are 0.023/Cu2, 0.019/Te1, 0.011/Cu1, and 0.0/Te2. The band character decomposition analysis as listed in Supporting Information, Table S3 indicates that the top three VBs are mainly composed from Cu2−3d, Te1−5p, and minor Cu1−3d. Consequently, the metallic conductivity of $Cs_3Cu_{20}Te_{13}$ originates mostly from the bands of Cu2, Te1 atoms constructing the sodalite framework with the contribution of Cu1 on the hexagonal ring of Cage-III; that is, the quite broad VBs near the Fermi level are mainly originated from the orbital interactions between $Cu2(Te1)_4$ tetrahedra.

The crystal orbital Hamilton population (COHP) was calculated to verify the bonding interactions (Figure 7). The

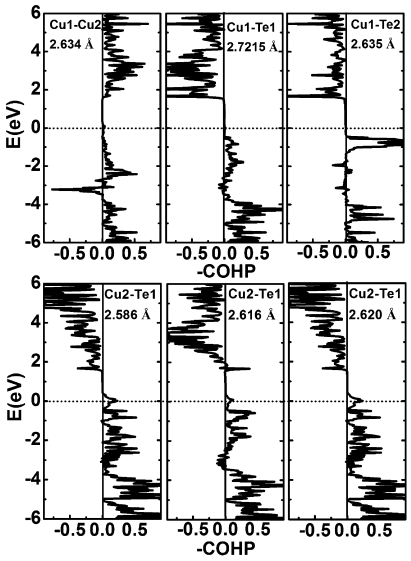

Figure 7. COHP curves of selected bond distances for $Cs_3Cu_{20}Te_{13}$. The E_F is set at 0 eV.

Cu1−Cu2 = 2.634 Å distance on the hexagonal rings of Cage-III is twice of the sum of the Slater radii (r_{Cu} = 1.35 Å[28]) and possesses an integrated crystal orbital Hamilton population (ICOHP) value of −0.64 eV, indicating a weak yet noticeable bonding interaction. The Cu2−Te1 bonds constructing the sodalite framework are strong covalent bonding interactions, and their bonding strength increases as the bond length decreases, as follows (length/ICOHP): 2.586 Å/−2.41 eV, 2.616 Å/−1.92 eV, 2.620 Å/−1.81 eV. The ICOHP of Cu1−Te2 bond (2.635 Å) within the guest Te2@$Cu1_8$ cube is −1.48 eV. Yet, these two types of bonding interactions are considerably stronger than that of Cu1−Te1 = 2.7215 Å/−1.34 eV on the hexagonal rings of Cage-III. As the COHP curves in Figure 7 show, the E_F cuts through the bonding interactions of Cu2−Te1, indicating a metal feature of the sodalite framework. On the contrary, the sharp bonding COHP peak of Te2−Cu1 is well below E_F, indicating the typical anion feature of $Te2^{2-}$. And the COHP of the secondary interaction Cu1−Te1 (2.7215 Å) and Cu1−Cu2 (2.634 Å) on the hexagonal rings of Cage-III show nonbonding interaction feature at E_F. Thus, to assign the Te2@$Cu1_8$ cube as a guest species is reasonable. Consequently, the formula of $Cs_3Cu_{20}Te_{13}$ can also be described as $(Cs^{1+})_3[(Cu1^{1+})_8(Te2)^{2-}][(Cu2Te1)_{12}]^{0.75-}$, which indicates that the sodalite framework is metallic $(CuTe)_{12}^{0.75-}$, which may due to the close electronegativities of Cu and Te atoms.[9] If more electrons can be introduced into the sodalite framework to push up the E_F about 0.5 eV, for example, by replacing Cs^+ with Ba^{2+}, the hypothetical $(Ba^{2+})_3(Cu^{1+})_{20}(Te^{2-})_{13}$ would be an electron-precise Zintl phase with a narrow band gap, which is predicted to be a good candidate for thermoelectric materials. This is worth trying.

EXPERIMENTAL SECTION

Syntheses. Reactants Pr (99.95%, Huhhot Jinrui Rare Earth Co., Ltd.), Cu and Te (99.99%, Alfa Aesar China (Tianjin) Co., Ltd.), and CsCl (99.9%, Jiangxi Dongpeng New Materials Co., Ltd.) were used as purchased and stored in an Ar-filled glovebox with controlled oxygen and moisture levels below 0.1 ppm.

A few single crystals of $Cs_3Cu_{20}Te_{13}$ were first obtained as byproducts (blue-black block-shaped crystals) from the reaction of $Cs_xPr_2Cu_{6-x}Te_6$ loaded with mole ratio of CsCl/Pr/Cu/Te = 3:2.4:5:6.[1] Single-crystal diffraction data generated the formula of $Cs_3Cu_{20}Te_{13}$. Subsequently, reactions loaded with CsCl/Pr/Cu/Te = 8:1:20:13 (1.476 g in total) were carried out in a silica crucible sealed in an evacuated silica jacket tube. The assembly was heated to 1123 K over 50 h, dwelt for 120 h, then slowly cooled to 723 K over 60 h and subsequently to 473 K within 70 h before the furnace was shut off. The raw products were washed with distilled water three times to remove the excess flux and the chloride byproducts and then dried with ethanol. Unfortunately this reaction did not yield the target compound; instead, $CsCu_{13}Te_6$ was the main product (Supporting Information, Figure S1).

First, it was clear that without Pr (as a reductive agent), the reaction of CsCl/Cu/Te = 8:17.5:13 could not produce the title compound (Supporting Information, Figure S3). Similar to those in $A_xRE_2Cu_{6-x}Te_6$[1] and $CsMnInTe_3$,[29] CsCl worked as a reactant as well as a flux assisting crystallization. Second, on the basis of many explorations, we realized that the loading amount of Cu was crucial for this reaction. For example, loading ratios of CsCl/Pr/Cu/Te = 8:1:17.5:13 generated the title compound with a high 93% yield. Keeping the other amounts fixed, increasing the Cu ratio to 17.75−19 generated $CsCu_{13}Te_6$ (with a higher Cu/Te ratio) as the impurity or even as the main product (Supporting Information, Figure S1). On the other hand, by decreasing the Cu ratio from 17.5 to the range of 16 to 17.25, binaries (such as $Cu_{2.86}Te_2$ with a lower Cu/Te ratio) together with unknown phases were found (Supporting Information, Figure S2).

The title compound $Cs_3Cu_{20}Te_{13}$ was stable in air over a period of months. The best yield of $Cs_3Cu_{20}Te_{13}$ is >94% with about 6% $Cu_{2.86}Te_2$ binary impurity by the reactions loaded with CsCl/Pr/Cu/Te = 8:1:17.5:13 ratios and a total amount of 1.423 g (Supporting Information, Figure S4). Since the color was distinct between the impurity $Cu_{2.86}Te_2$ (purple) and $Cs_3Cu_{20}Te_{13}$ (blue-black), the block-shaped target crystals were manually selected.

Single-Crystal Structure Analyses. The single-crystal X-ray diffraction data were collected on a Saturn 724 CCD diffractometer equipped with a graphite-monochromated Mo Kα radiation (λ = 0.71073 Å) at 293 K. The absorption corrections were done by the multiscan method. The space group $Fm\bar{3}$ (No. 202) was assigned according to the systematic absence, E-values statistics, which lead to subsequently successful structure refinement. The structure was solved by the direct method and refined by the full-matrix least-squares fitting on F^2 by SHELX-97.[30] All atoms were refined with anisotropic thermal parameters and secondary extinction corrections. The atomic coordinates were standardized with the STRUCTURE TIDY program.[31] Table 1 and Supporting Information, Table S2 list crystallographic data; additional structural data is listed in Table 2.

dx.doi.org/10.1021/ic500291v | Inorg. Chem. 2014, 53, 5575−5580

Table 1. Crystallographic Data and Structural Refinements for $Cs_3Cu_{20}Te_{13}$

formula	$Cs_3Cu_{20}Te_{13}$
formula weight	3328.33
space group	$Fm\bar{3}$
a (Å)	14.7557(6)
V (Å^3)	3212.8(2)
Z	4
temperature (K)	293(2)
ρ_{cal} (g/cm^3)	6.881
μ (Mo Kα)(mm^{-1})	27.841
$R1$, $wR2$ [$I > 2\sigma(I)$][a]	0.0424, 0.1198
$R1$, $wR2$ (all data)	0.0432, 0.1208
goodness of fit on F^2	1.075
largest diff. peak and hole (e Å^{-3})	3.52, −2.08

[a] $R_1 = \Sigma||Fo| - |Fc||/\Sigma|Fo|$, $wR_2 = [\Sigma w(Fo^2 - Fc^2)^2/\Sigma w(Fo^2)^2]^{1/2}$

Powder X-ray Diffraction. Powder X-ray diffraction data were measured at room temprature on a Rigaku Miniflex Π powder diffractometer, using monochromatized Cu Kα radiation in the 2θ range of 5−85° with scan step of 0.05°.

Elemental Analyses. Semiquantitative microprobe elemental analysis was performed on a field emission scanning electron microscope (FESEM, JSM6700F) equipped with an energy dispersive X-ray spectroscope (EDX, Oxford INCA). EDX was measured on visibly clean fresh-cut surfaces on the same $Cs_3Cu_{20}Te_{13}$ crystal used for the single-crystal diffraction data collection. The results indicated the presence of Cs, Cu, and Te without any other detectable elements, such as Pr or Cl. The EDX average atomic percentages (atom %) 8.1(2)/Cs, 55.7(9)/Cu, and 36.2(9)%/Te, agreed well with the single-crystal refinement results: 8.3, 55.6, and 36.1%. (Supporting Information, Figure S5 and Table S1).

Magnetic Property. Magnetic susceptibilities of $Cs_3Cu_{20}Te_{13}$ were measured on a Quantum Design PPMS-9T magnetometer at 2−300 K under a constant magnetic field of 1000 Oe. About 20−40 mg of hand-picked crystals were ground to fine powders and loaded into a gelatin capsule. Corrections for contributions from the container and the ion-core diamagnetism were applied.

Electrical Conductivity. Electrical conductivity was measured on a cold-pressed polycrystalline pellet (size ≈ 2.1 × 2.0 × 9.1 mm^3; density ≈ 78% of the theoretical one) on an ULVAC-RIKOZEM-3 instrument by the four-probe method under flowing Ar. The data were measured three times in the temperature range to ensure the reliability. After the measurement, the sample did not decompose, and no phase transition or significant impurity was observed by the XRD taken at this stage. (Supporting Information, Figure S6).

Theoretical Calculations. The electronic structures (band structures and density of states DOS) were calculated by Vienna ab initio simulation packages (VASP)[32] (Figure 6), and the COHP (Figure 7) was calculated by tight-binding linear muffin-tin orbital atomic sphere approximation (TB-LMTO-ASA) methods.[33,37] The VASP was based on the density functional theory using general gradient approximation (GGA-PBE) to treat the exchange and correlation potential.[34] And the projector augmented wave (PAW) was used as the plane wave basis.[35] The plane-wave cutoff energy was set at 425 eV and a grid of 9 × 9 × 9 Monkhurst-Pack[36] k-points was used for the self-consistent-field convergence of the total electronic energy. The Fermi level was set at zero as the energy reference.

The local density and atomic sphere approximations were used in the Stuttgart LMTO program.[33,37] Interstitial sphere was introduced to achieve space filling. The basis sets included 6s, 6p, and 5d functions for Cs; 4s, 4p, and 3d functions for Cu; 5s, 5p, 4d, and 4f functions for Te; and s, p, and d functions for "empty spheres" (ES). The k-space integrations were performed by tetrahedral method. The Fermi level was set at zero as the reference of the energy.

CONCLUSION

The first sodalite-type telluride, $Cs_3Cu_{20}Te_{13}$, was synthesized and well-characterized. Its 3D sodalite framework is constructed by $(CuTe)_{12}$ tetrakaidecahedra, each of which encapsulates a different guest species, either a Cs^+ or a Te@Cu_8 cube, leading to a fully expanded 2 × 2 × 2 supercell with respect to that of a conventional sodalite. The single-crystal analyses, together with DFT analyses, conclude that the formula can be written as $(Cs^{1+})_3[(Cu1^{1+})_8(Te2)^{2-}][(Cu2Te1)_{12}]^{0.75-}$, indicating the electron deficiency that agrees well with the Pauli paramagnetism and the metallic conductivity experimental results. The DFT calculations also reveal the electron deficiency originating from the Cu 3d and Te 5p states near E_F and the unique feature of the metallic sodalite framework accommodating anionic guest species. Theoretical analyses also point out that the hypothetic derivative $Ba_3Cu_{20}Te_{13}$ should be an electron-precise Zintl phase having a desirable narrow band gap of 0.5 eV and consequently may show promising thermoelectric property.

ASSOCIATED CONTENT

Supporting Information

The additional crystallographic data and CIF file, together with additional tables and figures. This material is available free of charge via the Internet at http://pubs.acs.org.

AUTHOR INFORMATION

Corresponding Author

*Email: liming_wu@fjirsm.ac.cn.

Notes

The authors declare no competing financial interest.

ACKNOWLEDGMENTS

This research was supported by National Natural Science Foundation of China under Projects (20973175, 21233009), and NSF of Fujian Province (2011J05036). We thank Prof. Xiao-Ying Huang at FJIRSM for helpful discussions on the crystal structure refinement.

Table 2. Atomic Coordinates and Equivalent Isotropic Displacement Parameters of $Cs_3Cu_{20}Te_{13}$

atom	Wyckoff site	x	y	z	U_{eq} (Å)[a]
Cs1	8c	0.25	0.25	0.75	0.0260(6)
Cs2	4b	0	0.5	0	0.0286(7)
Cu1	32f	0.103 11(8)	0.103 11(8)	0.103 11(8)	0.0321(6)
Cu2	48h	0	0.2470(2)	0.1262(2)	0.0270(6)
Te1	48h	0.124 67(5)	0.254 51(5)	0	0.0176(4)
Te2	4a	0	0	0	0.0201(6)

[a] $U_{(eq)}$ is defined as one-third of the trace of the orthogonalized U_{ij} tensor.

dx.doi.org/10.1021/ic500291v | Inorg. Chem. 2014, 53, 5575−5580

REFERENCES

(1) Meng, C. Y.; Chen, H.; Wang, P.; Chen, L. *Chem. Mater.* **2011**, *23*, 4910−4919.
(2) Jacyna-Onyszkiewicz1, I.; Sidowski, M.; Starodub, V.; Robaszkiewicz, S. *Phys. Status Solidi A* **2003**, *196*, 271−274.
(3) Axtell, E. A.; Park, Y.; Chondroudis, K.; Kanatzidis, M. G. *J. Am. Chem. Soc.* **1998**, *120*, 124−136.
(4) Androulakis, J.; Peter, S. C.; Li, H.; Malliakas, C. D.; Peters, J. A.; Liu, Z. F.; Wessels, B. W.; Song, J. H.; Jin, H.; Freeman, A. J.; Kanatzidis, M. G. *Adv. Mater.* **2011**, *23*, 4163−4167.
(5) Peplinski, Z.; Brown, D. B.; Watt, T.; Hatfield, W. E.; Day, P. *Inorg. Chem.* **1982**, *21*, 1752−1755.
(6) Zhang, X.; Kanatzidis, M. G. *J. Am. Chem. Soc.* **1996**, *118*, 693−694.
(7) (a) Ruädorff, W.; Schwarz, H. G.; Walter, M. *Z. Anorg. Allg. Chem.* **1952**, *269*, 141−152. (b) Brown, D. B.; Zubieta, J. A.; Vella, P. A.; Wrobleski, J. T.; Watt, T.; Hatfield, W. E.; Day, P. *Inorg. Chem.* **1980**, *19*, 1945−1950. (c) Klepp, K.; Boller, H.; Völlenkle, H. *Monatsh. Chem.* **1980**, *111*, 727−733. (d) Burschka, C. *Z. Anorg. Allg. Chem.* **1980**, *463*, 65−71.
(8) (a) Burschka, C. *Z. Naturforsch.* **1979**, *B34*, 675−677. (b) ter Haar, L. W.; Di Salva, F. J.; Bair, H. E.; Fleming, R. M.; Waszczak, J. V.; Hatfield, W. E. *Phys. Rev. B* **1987**, *35*, 1932−1938. (c) Schils, H.; Bronger, W. *Z. Anorg. Allg. Chem.* **1979**, *456*, 187−193.
(9) Park, Y.; Degroot, D. C.; Schindler, J.; Kannewurf, C. R.; Kanatzidis, M. G. *Angew. Chem., Int. Ed. Engl.* **1991**, *30*, 1325−1328.
(10) Zhang, X.; Park, Y. B.; Hogan, T.; Schindler, J. L.; Kannewurf, C. R.; Seong, S.; Albright, T.; Kanatzidis, M. G. *J. Am. Chem. Soc.* **1995**, *117*, 10300−10310.
(11) Park, Y.; Kanatzidis, M. G. *Chem. Mater.* **1991**, *3*, 781−783.
(12) Emirdag, M.; Schimek, G. L.; Kolis, J. W. *J. Chem. Soc., Dalton Trans.* **1999**, 1531−1532.
(13) Chen, X.; Huang, X.; Li, J. *Inorg. Chem.* **2001**, *40*, 1341−1346.
(14) Depmeier, W. *Rev. Mineral. Geochem.* **2005**, *57*, 203−240.
(15) Richardson, J. W.; Pluth, J. J.; Smith, J. V.; Dytrych, W. J. *J. Phys. Chem.* **1988**, *92*, 243−247.
(16) Zhang, R. C.; Zhang, C.; Zhang, D. J.; Wang, J. J.; Zhang, Z. F.; Ji, M.; An, Y. L. *Z. Anorg. Allg. Chem.* **2012**, *638*, 2503−2507.
(17) Kirsanova, M. A.; Olenev, A. V.; Abakumov, A. M.; Bykov, M. A.; Shevelkov, A. V. *Angew. Chem., Int. Ed.* **2011**, *50*, 2371−2374.
(18) Santamaría-Pérez, D.; Liebau, F. *Struct. Bonding (Berlin, Ger.)* **2011**, *138*, 1−29.
(19) Bode, H.; Teufer, G. *Acta Crystallogr.* **1955**, *8*, 611−614.
(20) Wartchow, R. *Z. Kristallogr.—New Cryst. Struct.* **1997**, *212*, 80−80.
(21) Zintl, E. *Angew. Chem.* **1939**, *52*, 1−6.
(22) Nesper, R. *Prog. Solid State Chem.* **1990**, *20*, 1−45.
(23) Nesper, R. *Angew. Chem., Int. Ed. Engl.* **1991**, *30*, 789−817.
(24) Peplinski, Z.; Brown, D. B.; Watt, T.; Hatfield, W. E.; Dayic, P. *Inorg. Chem.* **1982**, *21*, 1752−1755.
(25) Calta, N. P.; Kanatzidis, M. G. *Inorg. Chem.* **2013**, *52*, 9931−9940.
(26) Xia, S. Q.; Bobev, S. *J. Am. Chem. Soc.* **2007**, *129*, 10011−10018.
(27) Malliakas, C. D.; Kanatzidis, M. G. *J. Am. Chem. Soc.* **2007**, *129*, 10675−10677.
(28) Slater, J. C. *J. Chem. Phys.* **1964**, *41*, 3199−3204.
(29) Lin, H.; Shen, J. N.; Chen, L.; Wu, L. M. *Inorg. Chem.* **2013**, *52*, 10726−10728.
(30) Sheldrick, G. M. *SHELXTL*, version 5.1; Bruker-AXS: Madison, WI, 1998.
(31) Gelato, L. M.; Parthe, E. *J. Appl. Crystallogr.* **1987**, *20*, 139−143.
(32) Kresse, G.; Furthmüller. *J. Phys. Rev. B* **1996**, *54*, 11169−11186.
(33) Tank, G.; Jepsen, O.; Burkhardt, A.; Andersen, O. K. *The TB-LMTO-ASA program*, version 4.7; Max-Planck-Institut für Festkörperforschung: Stuttgart, Germany, 1998.
(34) Perdew, J. P.; Burke, K.; Ernzerhof, M. *Phys. Rev. Lett.* **1996**, *77*, 3865−3868.
(35) Kresse, G.; Joubert, D. *Phys. Rev. B* **1999**, *59*, 1758−1775.
(36) Monkhorst, H. J.; Pack, J. D. *Phys. Rev. B* **1976**, *13*, 5188−5192.
(37) Kovnir, K. A.; Shevelkov, A. V. *Russ. Chem. Rev.* **2004**, *73*, 923−938.